ORGANIC CHEMISTRY FRONTIERS

RESEARCH ARTICLE

View Article Online
View Journal

Cite this: DOI: 10.1039/d3qo01914d

Using pyrrolizine-fused bipolar PAHs as a new strategy towards efficient red and NIR emissive dyes†

Krzysztof Bartkowski, ‡[a] Abhishek Kumar Gupta, ‡[b] Tomas Matulaitis,[b] Maja Morawiak,[a] Eli Zysman-Colman *[b] and Marcin Lindner *[a]

Received 17th November 2023,
Accepted 2nd December 2023

DOI: 10.1039/d3qo01914d

rsc.li/frontiers-organic

We report the synthesis and characterization of the first pyrrolizine-embedded PAH systems. The bipolar core, based on a naphthalimide and indole fusion, was successfully synthesized through a one-pot cascade of Suzuki/Boc deprotection/Buchwald–Hartwig transformations. A facile post-functionalization of the unoccupied β-position of the heterocycle with aromatic amines as donor subunits led to a set of donor–acceptor architecture-based dyes. Effective narrowing of the HOMO–LUMO gap, along with its tuning by changing donor strength together with stabilization of π conjugation within the pyrrolizine–NMI core, provided a route to near-infrared (NIR) emission not only in solution (~740 nm) but also in the solid-state (~700 nm).

Nitrogen-doped polycyclic aromatic hydrocarbons (PAHs) that comprise N-pyrrolic fragments at the central or peripheral position of the π-extended structures[1] have recently attracted attention because of their distinctive geometry[2] and self-assembly behaviour,[3,4] their capability to strongly bind fullerenes,[5] their low oxidation potential,[6] and their high-charge carrier mobility.[7] Accordingly, pyrrole, pyrrolo[3,2-*b*]pyrrole,[2–5,7] as well as their azacoronene (in neutral or cationic forms)[6,8] and thiepine[7] fused PAH analogues have served as components for application in sensing,[5] photovoltaics,[9] liquid crystals,[6] and single-crystal field effect transistors,[7] respectively. Despite their highly conjugated structure, N-doped PAHs are typically only modestly emissive. A potential solution to this challenge is to integrate N-doped PAHs with electron-deficient segments. From the viewpoint of optical properties, this type of molecular design should lead to narrowed HOMO–LUMO gaps, lower energy excited states, and improved charge transport (CT) properties. In this context, two major molecular design strategies have been proposed so far: an initially proposed design encompasses N-heteroannulated perylene bisimides (PDIs) and the later one with thoroughly fused bipolar Naphthalene-1,8-dicarboximide (NMIs), as demonstrated in Fig. 1 (I and II), respectively. In line with these considerations, using a π-extended PDI scaffold with a highly reactive bay-region proved beneficial for incorporating an electron-rich, pyrrolic fragment (Fig. 1, Ia). This was achieved through regioselective nitration of PDI, followed by electrophilic Cadogan-type cyclization and alkylation/arylation reactions.[10] Such a readily available platform underwent various post-functionalizations, resulting in 1,3/1,4-phenyl-linked derivatives,[11–13] homo-coupled PDIs,[10] or thiophene-bridged thoroughly conjugated polycyclic aromatic hydrocarbons (PAHs)[14] with high π-electron density.

Regardless of the type of derivatization performed, these moieties exhibited a planar geometry that fosters a strong packing arrangement (even though double N-annulated species adopted a bowl-like geometry as displayed in Fig. 1, Ib)[15] which is detrimental from the viewpoint of emissive properties. Instead, N-annulated PDIs were successfully exploited as non-fullerene acceptors for organic solar cells. In a similar fashion, but creating a 7-membered, azepine-bridged PDI (see Fig. 1, Ic), Shinokubo and co-workers[16] presented a twisted species which in spite of possessing the desired non-planar arrangement shows modest optical features. Facing this challenge, very recently the second approach in which an electron-rich system is thoroughly fused and conjugated with an electron-poor moiety has also been demonstrated by our group (Fig. 1, IIa); that is, we showed the formation of a PAH consisting of 1,8-NMI and 3,6-di-*tert*-butylcarbazole (d*t*BuCz) *via* a

[a]*Institute of Organic Chemistry, Polish Academy of Sciences, Kasprzaka 44/52, 01-224 Warsaw, Poland*
[b]*Organic Semiconductor Centre, EaStCHEM School of Chemistry, University of St Andrews, St Andrews, UK*

†Electronic supplementary information (ESI) available: Experimental procedures for the syntheses of materials, spectroscopy data of new compounds, single crystal X-ray crystallographic data, cyclic voltammogram, the copies of NMR spectra of new compounds, and theoretical calculation details. CCDC 2216025–2216027, 2290709 and 2290710. For ESI and crystallographic data in CIF or other electronic format see DOI: https://doi.org/10.1039/d3qo01914d

‡These authors contributed equally.

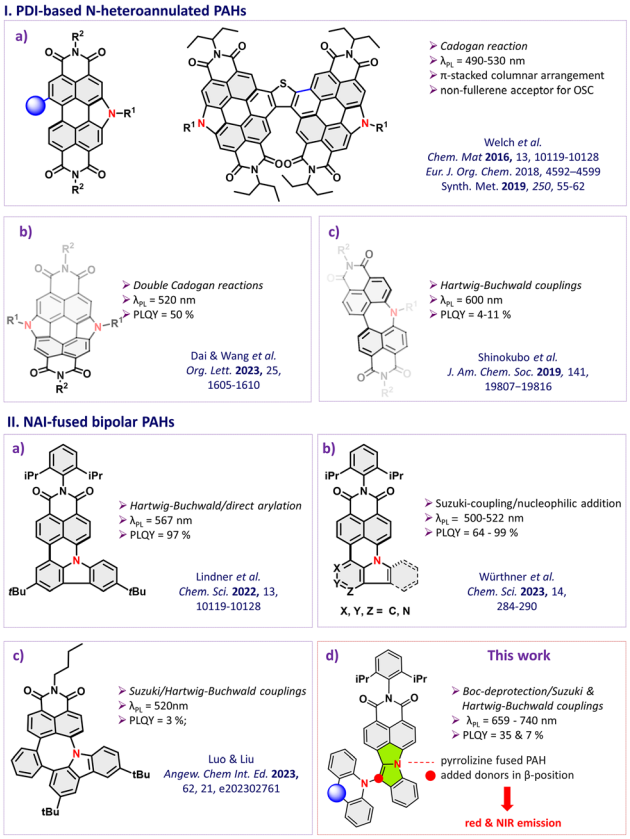

Fig. 1 Current progress in the domain of nitrogen-doped bipolar PAHs based on PDI N-heteroannulated systems (I a–c) and NMI-scaffolds (II a–c) fused within 6 and 7-membered rings; (d) novel approach toward double 5-membered rings based on pyrrolizine fused NMIs towards efficient red & NIR emitting systems.

6-membered ring closure utilizing one-pot Pd-catalysed cascade transformations encompassing the formation of C–N/C–C bonds by virtue of Buchwald–Hartwig cross-coupling/direct arylation reactions (Fig. 1, IIa).[17] This compound is very bright (PLQY ~ 95%). We demonstrated its utility as a terminal emitter in a so-called hyperfluorescent OLED that showed a maximum external quantum efficiency of 26%. Shortly after, Würthner and co-workers[18] reported another approach for synthesizing similar types of annulated compounds that were accessed following a cascade of Suzuki cross-coupling/nucleophilic addition reactions that emit in the green region with moderate-to-high PLQY (Fig. 1, IIb). In a similar fashion, but with 8*H*-benzo[3,4][1,2]azaborinino[5,6,1-*jk*]carbazole-8-ol as a precursor, Luo and Liu[19] reported a route to compounds containing a 7-membered ring consisting of a combination of Suzuki coupling and Buchwald–Hartwig amination reactions, as demonstrated in Fig. 1, IIc. Notably, all of these structures contain highly conjugated ambipolar architectures that are emissive as a result of the presence of a low-lying charge-transfer excited state. Thus, modification of their electron-rich segment is envisaged as a route to developing compounds that should emit in the red and NIR regions.

Here, we report a straightforward synthesis of the first example of fused NMI and pyrrolizine fragments, in which the β-position (see Fig. 1, IId) is functionalized with a set of electron-rich donor moieties, allowing us to establish an efficient approach toward a new family of highly emissive green-to-NIR dyes.

The synthesis of **3a–c** was accomplished in a three-step sequence (Scheme 1). We first tried to react *N*-(2,6-diisopropylphenyl)-4,5-bromo-NMI with unsubstituted indole; however, this approach failed to provide compound **1**. We next employed *N*-Boc-indole-2-boronic acid as a precursor. To enable the thermal decomposition of the Boc protecting group, the temperature of the reaction was increased, which proved to be the key to the sequential Buchwald–Hartwig amination and direct arylation, leading to fused intermediate **1** in 40% yield. With this in hand, its bromination led to **2** in quantitative yield, which was employed in a Buchwald–Hartwig amination with d*t*BuCz, 9,9-dimethyl-9,10-dihydroacridine (DMAc) and phenoxazine (PXZ) donor moieties. Dyes **3a–c** were obtained in moderate yields ranging from 30–45%. The structures of all intermediates and target compounds **3a–c** were unambiguously verified using ^{1}H NMR and ^{13}C NMR spectroscopy and HRMS (see the ESI† for more details). To gain more insights into the solid-state structure of these dyes, X-ray quality, single crystal structures were obtained for compounds **1** and **3c** by slow evaporation from solutions of DCM and chloroform, respectively (Fig. 2A and B). Compound **1** crystalized in the triclinic $P\bar{1}$ space group with two molecules per unit cell adopting antiparallel orientation of neighbouring molecules (Fig. 2A). Short intermolecular distances (3.52 Å) exist in the crystalline phase of unfunctionalized **1**, which imply strong π–π interactions between head-to-tail arranged

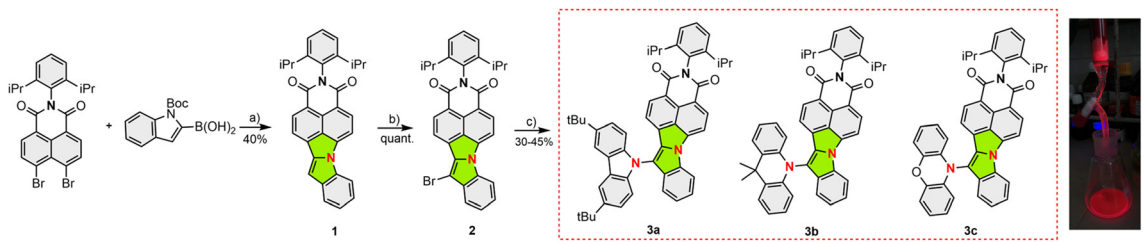

Scheme 1 The synthesis path towards emitters **3a–c** and red-emission of **3c** visible during purification. Reaction conditions: (a) Pd(P*t*Bu$_3$)$_2$, NaO*t*Bu, toluene, 120 °C, 72 h; (b) NBS, DMF, 12 h, RT; (c) R^{2}NH, Pd(P*t*Bu$_3$)$_2$, NaO*t*Bu, toluene, 120 °C, 24 h.

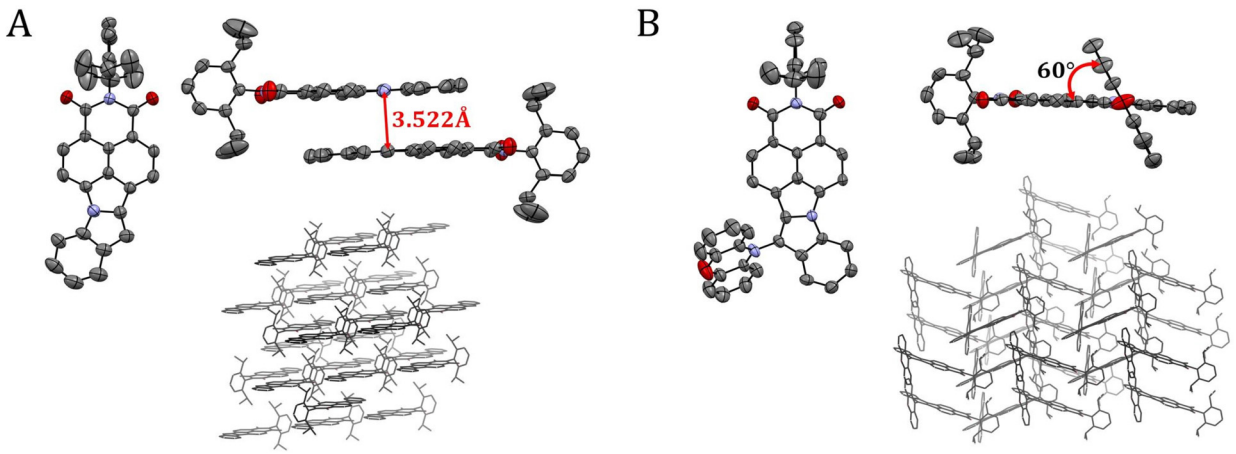

Fig. 2 X-ray structures and their packing of (A) **1** and (B) **3c**. The thermal ellipsoids are shown at 50% probability. The hydrogen atoms and solvent molecules have been removed for clarity.

molecules (Fig. 2A). Compound **3c** crystallized in monoclinic $P2_1$, also with two molecules per unit cell. The presence of the twisted quasi-axial PXZ donor (60°, Fig. 2B) influences the interactions in the crystal structure, which is reflected in the prevention of π-stack creation (Fig. S15†).

To gain insight into the photophysical behaviour of these compounds, we computationally modelled their structure and properties using density functional theory (DFT) at the PBE0/6-31G(d,p)[20] level of theory in the gas phase. Compound **1** possesses a structure where the central "pyrrolizine-fused-NMI (PF-NMI)" core is planar, while the diisopropylphenyl moiety is attached orthogonally (dihedral angle > 89°) to the PF-NAI group (Fig. S10†). Compounds **3a–c** possess a similar structure, but with the decorated donors adopting a twisted conformation with respect to the PF-NAI plane. The dihedral angle between the donor and PF-NAI plane is 50.8° in **3a**, 67.4° in **3b** and 60.4° in **3c** (Fig. S10†); the computed structure broadly matches with that observed in the crystal structure of **3c**.

The HOMO and LUMO of **1** are both delocalized across the PF-NMI core, with respective energies of −6.02/−2.77 eV. In **3a–c**, the LUMOs are mainly located on the fused-NMI core and have comparable energies of −2.76, −2.81 and −2.83 eV, respectively, while the HOMOs are increasingly localized on the donor substituent.

The HOMO levels reflect the relative strength of the donor substituent, with the HOMO of **3c** (−5.23 eV) being destabilized in comparison to those of both **3a** (−5.56 eV) and **3b** (−5.40 eV) because of the presence of stronger PXZ. The computed HOMO–LUMO gaps of **1**, **3a**, **3b** and **3c** are 3.25, 2.80, 2.59 and 2.40 eV, respectively (Fig. 3). This trend in HOMO–LUMO gaps is reflected in the S_1 and T_1 energies. The S_1 and T_1 energies of **1** are 2.88 eV and 1.84 eV, respectively, which are

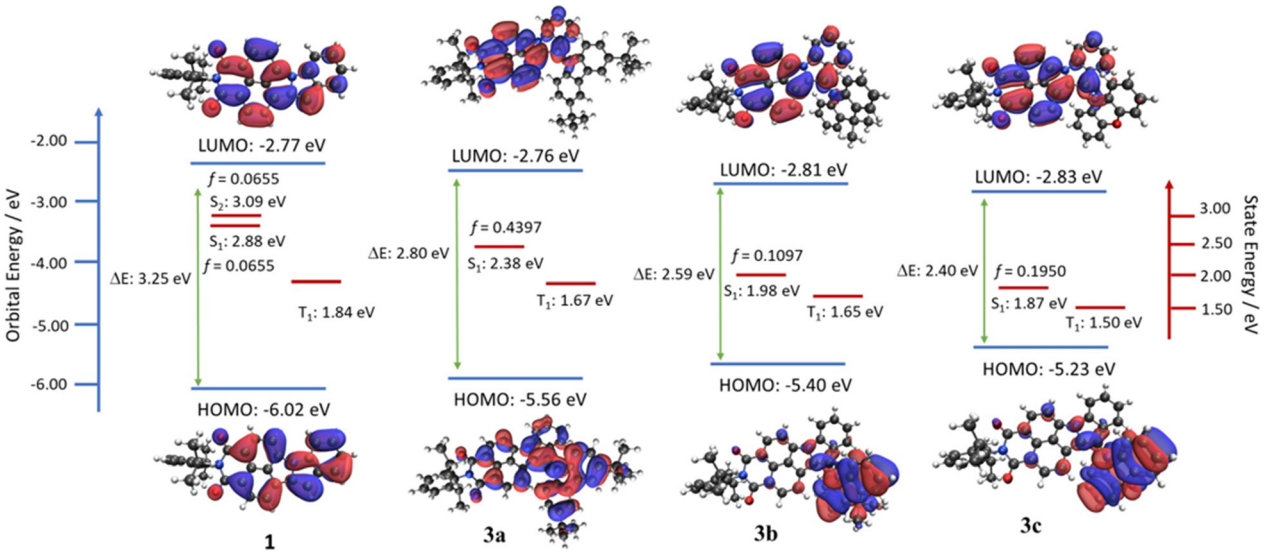

Fig. 3 Theoretical modelling of the energies of the HOMO/LUMO and the S_1 and T_1 states of **1** and **3a–c**.

stabilized to 2.38 and 1.67 eV for **3a**, 1.98 and 1.65 eV for **3b**, and 1.87 and 1.50 eV for **3c**. The calculated ΔE_{ST} values of **1** (1.04 eV) and **3a** (0.71 eV) are much larger than those of **3b** (0.33 eV) and **3c** (0.37 eV). These large singlet–triplet gaps almost certainly preclude that these compounds would show TADF behaviour. The oscillator strength (f) of the $S_0 \rightarrow S_1$ transition is higher at 0.4397 for **3a** in comparison to **3b** (0.1097), **3c** (0.1950) and **1** (0.0655), reflecting the larger overlap of the frontier molecular orbitals (FMOs) in **3a**.

The experimental HOMO and LUMO energies were deduced from electrochemistry, using cyclic and differential pulse voltammetry (CV and DPV) in DCM (Fig. 4 and Table 1). The electrochemical data were referenced to Fc/Fc^+ and are reported relative to a saturated calomel electrode (SCE). All compounds show two highly reversible reduction waves at around −1.0 and −1.46 V, which were assigned to successive reductions of the PF-NMI acceptor. Compound **1** shows a quasi-reversible oxidation wave at 1.43 V, assigned to oxidation of the whole molecule. Compounds **3a–c** show two reversible oxidation waves: the first wave is associated with oxidation of the donor moiety and the second one is associated with oxidation of the pyrrolizine-attached diisopropylphenyl moiety. The oxidation/reduction potentials of **1**, **3a**, **3b** and **3c** were determined from the first oxidation/reduction peaks from DPV and they are 1.43/−1.01, 1.16/−0.94 V, 1.07/−0.97 V, and 0.89/−0.93 V, respectively (Fig. 4). Based on these data, HOMO/LUMO values were determined to be −5.77/−3.33 eV, −5.49/−3.40 eV, −5.41/−3.37 and −5.23/−3.41 eV for **1**, **3a**, **3b**, and **3c**, respectively (Table 1) and the estimated electrochemical band gaps were 2.44, 2.09, 2.04, and 1.82 eV respectively, which align with the trend observed from the DFT calculations.

We performed photophysical measurements of compounds **1** and **3a–c** to understand their ground- and excited-state behaviour. Compound **1** shows a single strong absorption band at 480 nm (ε = 39.4 × 10^3 M^{-1} cm^{-1}) in toluene (Fig. 5).

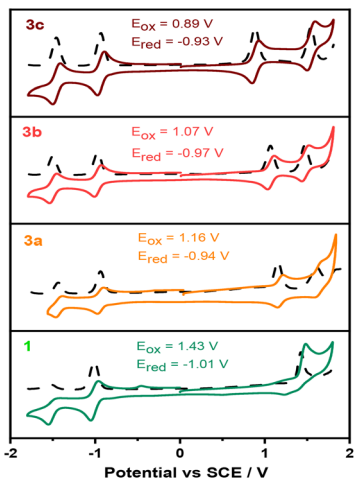

Fig. 4 Cyclic and differential pulse voltammograms of **1**, **3a**, **3b**, and **3c** in degassed DCM (scan rate = 100 mV s^{-1}).

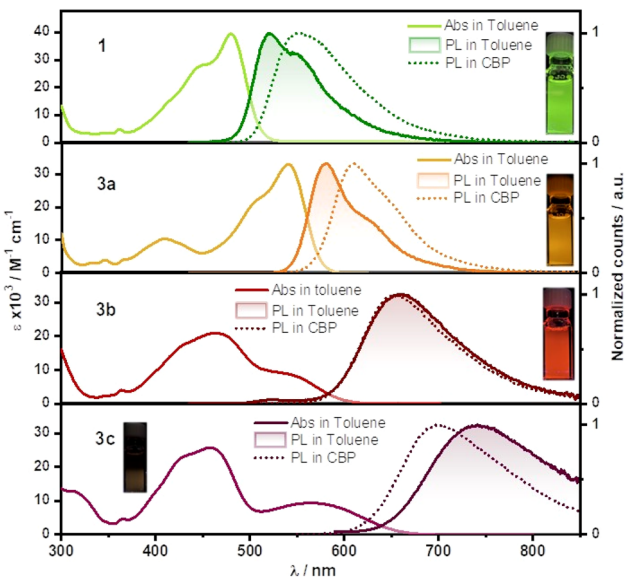

Fig. 5 Molar absorptivity of **1** and **3a–c** in toluene and photoluminescence spectra of **1** and **3a–c** in toluene (λ_{exc} = 420 nm for **1**, 480 nm for **3a**, and 500 nm for **3b** and **3c**) and 5 wt% doped samples in CBP (λ_{exc} = 340 nm).

Table 1 Photophysical properties of **1**, **3a**, **3b** and **3c**

			Toluene				5% in CBP		
Compound	HOMO[a]/eV	LUMO[a]/eV	λ_{UV}[b]/nm (ε/×10^3 M^{-1} cm^{-1})	λ_{PL}[b]/nm	τ[c]/ns	Φ_{PL}[d]/%	λ_{PL}[e]/nm	Φ_{PL}/% air/N_2[f]	τ_{avg}[g]/ns
1	−5.77	−3.33	480 (39.4)	521	8.3	42	552	33/34	17.3
3a	−5.49	−3.40	409, 540 (33.1)	580	7.6	83	610	68/68	7.0
3b	−5.41	−3.37	463 (20.9), 548	659	8.9	22	654	34/35	11.6
3c	−5.23	−3.41	458 (25.7), 568	741	0.8	1	700	7/7	3.1

[a] $E_{HOMO/LUMO} = -(E^{ox}/E^{red} + 4.8)$ eV,[21] where E^{ox} is the anodic peak potential and E^{red} is the cathodic peak potential calculated from DPV in relation to Fc/Fc^+ as the internal reference and referenced *versus* SCE (0.46 V *vs.* SCE)[22,23] in DCM with 0.1 M $[^nBu_4N]PF_6$ as the supporting electrolyte. [b] At 298 K, values quoted are in solutions under N_2, which were prepared by three freeze–pump–thaw cycles (λ_{exc} = 420 nm for **1**, 480 nm for **3a**, and 500 nm for **3b** and **3c**). [c] λ_{exc} = 374 nm. [d] At 298 K, values quoted are in solutions under air. [e] Thin films were prepared by spin-coating 5 wt% doped samples in 4,4′-bis(*N*-carbazolyl)-1,1′-biphenyl (CBP) (λ_{exc} = 340 nm). [f] Photoluminescence quantum yields of the thin films were determined using an integrating sphere (λ_{exc} = 305 nm or 340 nm) under air and N_2 atmosphere at 298 K. [g] Time-resolved PL decays were recorded at 298 K under an O_2-free atmosphere (λ_{exc} = 374 nm). Average lifetime ($\tau_{avg} = \sum A_i\tau_i^2/\sum A_i\tau_i$), where A_i is the pre-exponential for lifetime (τ_{avg}).

DFT predicts this band to reflect a mixture of locally excited (LE) π–π* and charge transfer (CT) transitions because of the ambipolar nature of PF-NMI, which correlate with the high oscillation strength (f = 0.5305) of the $S_0 \rightarrow S_2$ transition; however, the oscillation strength of $S_0 \rightarrow S_1$ is very low 0.0655 (Fig. S11 and Table S1†) and so this band likely reflects a combination of these two transitions. In compound **3a**, the low-energy absorption band is bathochromically shifted at 540 nm ($\varepsilon = 33.1 \times 10^3$ M^{-1} cm^{-1}) and has the same profile as that in **1** where the transitions are of mixed LE/CT character (f = 0.4397). The absorption profiles of **3b**and **3c** are more complex. The low energy bands at 548 nm and 568 nm, respectively, reflect a CT transition from the donor to PF-NMI (Fig. S11 and Table S1†). The high energy bands (and associated high-energy shoulder) at 463 nm ($\varepsilon = 20.9 \times 10^3$ M^{-1} cm^{-1}) for **3b** and at 458 nm ($\varepsilon = 25.7 \times 10^3$ M^{-1} cm^{-1}) for **3c** (Table 1) are assigned to the absorption of the PF-NAI core as the profile grossly aligns with that of **1** and the band is only modestly blue-shifted by about 20 nm.

The parent compound **1** shows (Fig. 5) structured photoluminescence in toluene at λ_{PL} of 521 nm, indicative of emission from an LE state, and has a Φ_{PL} of 42%. Compound **3a** has a similar emission profile that is red-shifted at λ_{PL} of 581 nm, aligning with that predicted by DFT; however, the Φ_{PL} is much higher at 83%. The emission profiles of **3b** and **3c** are distinctly red-shifted and unstructured at 659 nm (deep-red) and 741 nm (NIR), reflecting emission from a CT state (Fig. 5 and Table 1). The Φ_{PL} decreases to 21.6% and 1.1% for **3b** and **3c**, respectively (Table 1); this is due to the lower oscillator strength associated with the CT transition and to the energy gap law.[24,25] All emitters showed mono-exponential decay kinetics with photoluminescence lifetimes (τ_{PL}) of 8.3 ns for **1**, 7.6 ns for **3a**, 8.9 ns for **3b** and 0.8 ns for **3c** in toluene (Table 1 and Fig. S13†). All emitters exhibit positive solvatochromism; however, the degree of solvatochromism significantly increases from **1** (65 nm) to **3c** (149 nm), which demonstrates that **1** and **3a** have emissive excited states of mixed LE/CT character while the excited states of **3b** and **3c** are of CT character (Fig. S12†). We also investigated the PL behaviour of these emitters in the solid state (Fig. 5) by doping 5 wt% **1** and **3a–c** in 4,4′-bis(*N*-carbazolyl)-1,1′-biphenyl (CBP). Surprisingly, the emission of compounds **1** and **3a** was approximately 30 nm red-shifted to 552 and 610 nm (the structured emission, though less resolved is still present) while the Φ_{PL} decreased (34% for **1** and 68% for **3a**) relative to the measurements in toluene (Table 1). In contrast, the emission of **3b** and **3c** was blue-shifted to 654 and 700 nm, respectively, while the Φ_{PL} increased to 35% for **3b** and to 7% for **3c**. All compounds showed multi-exponential decay kinetics, with average lifetimes τ_{PL} of 17.3 ns for **1**, 7.0 ns for **3a**, 11.6 ns for **3b** and 3.1 ns for **3c** (Table 1).

In summary, we report a one-pot cascade cyclization resulting in fully conjugated pyrrolizine-fused NMI scaffolds, which upon facile post-functionalization with a set of electron-rich substituents deliver red and NIR emissive properties (<700 nm) both in solution and in the solid state. The demonstrated design should enable further modifications, opening a new avenue for their use as NIR-emissive materials in opto-electronic devices which is the current subject of our studies.

Conflicts of interest

There are no conflicts to declare.

Acknowledgements

K. B. and M. L. acknowledge support from the National Centre for Research and Development, Poland, Grant No. LIDER/21/0077/L-11/19/NCBR/2020. M. L. is a recipient of a scholarship awarded by the Polish Ministry of Education and Science to outstanding young scientists (2/DSP/2021). The St Andrews team thanks the Leverhulme Trust (RPG-2022-032) and the Engineering and Physical Sciences Research Council (EP/R035164/1, EP/W007517) for support.

Notes and references

1 A. Borissov, Y. K. Maurya, L. Moshniaha, W.-S. Wong, M. Żyła-Karwowska and M. Stępień, Recent Advances in Heterocyclic Nanographenes and Other Polycyclic Heteroaromatic Compounds, *Chem. Rev.*, 2022, **122**(1), 565–788.

2 Y. Tokimaru, S. Ito and K. Nozaki, A Hybrid of Corannulene and Azacorannulene: Synthesis of a Highly Curved Nitrogen-Containing Buckybowl, *Angew. Chem., Int. Ed.*, 2018, **57**(31), 9818–9822.

3 K. Nakamura, K. Ochiai, A. Yubuta, D. He, D. Miyajima and S. Ito, Pyridine-Fused Azacorannulene: Fine-Tuning of the Structure and Properties of Nitrogen-Embedded Buckybowls, *Precis. Chem.*, 2023, **1**(1), 29–33.

4 M. Krzeszewski, Ł. Dobrzycki, A. L. Sobolewski, M. K. Cyrański and D. T. Gryko, Bowl-Shaped Pentagon- and Heptagon-Embedded Nanographene Containing a Central Pyrrolo[3,2-*b*]Pyrrole Core, *Angew. Chem., Int. Ed.*, 2021, **60**(27), 14998–15005.

5 H. Yokoi, Y. Hiraoka, S. Hiroto, D. Sakamaki, S. Seki and H. Shinokubo, Nitrogen-Embedded Buckybowl and Its Assembly with C60, *Nat. Commun.*, 2015, **6**(1), 8215.

6 L. Delage-Laurin and T. M. Swager, Liquid Crystalline Magneto-Optically Active Peralkylated Azacoronene, *JACS Au*, 2023, **3**(7), 1965–1974.

7 W. Wang, F. Hanindita, Y. Tanaka, K. Ochiai, H. Sato, Y. Li, T. Yasuda and S. Ito, Π-Extended Pyrrole-Fused Heteropine: Synthesis, Properties, and Application in Organic Field-Effect Transistors, *Angew. Chem., Int. Ed.*, 2023, **62**(8), e202218176.

8 M. Żyła, E. Gońka, P. J. Chmielewski, J. Cybińska and M. Stępień, Synthesis of a Peripherally Conjugated 5-6-7 Nanographene, *Chem. Sci.*, 2016, **7**(1), 286–294.

9 L. Wang, L. Lin, J. Yang, Y. Wu, H. Wang, J. Zhu, J. Yao and H. Fu, Singlet Fission in a Pyrrole-Fused Cross-Conjugated

Skeleton with Adaptive Aromaticity, *J. Am. Chem. Soc.*, 2020, **142**(23), 10235–10239.

10 A. D. Hendsbee, J.-P. Sun, W. K. Law, H. Yan, I. G. Hill, D. M. Spasyuk and G. C. Welch, Synthesis, Self-Assembly, and Solar Cell Performance of N-Annulated Perylene Diimide Non-Fullerene Acceptors, *Chem. Mater.*, 2016, **28**(19), 7098–7109.

11 Z. Ma, H. Fu, D. Meng, W. Jiang, Y. Sun and Z. Wang, Isomeric N-Annulated Perylene Diimide Dimers for Organic Solar Cells, *Chem.– Asian J.*, 2018, **13**(8), 918–923.

12 M. Vespa, J. R. Cann, S. V. Dayneko, O. A. Melville, A. D. Hendsbee, Y. Zou, B. H. Lessard and G. C. Welch, Synthesis of a Perylene Diimide Dimer with Pyrrolic N–H Bonds and N-Functionalized Derivatives for Organic Field-Effect Transistors and Organic Solar Cells, *Eur. J. Org. Chem.*, 2018, 4592–4599.

13 L. Rocard, D. Hatych, T. Chartier, T. Cauchy and P. Hudhomme, Original Suzuki–Miyaura Coupling Using Nitro Derivatives for the Synthesis of Perylenediimide-Based Multimers, *Eur. J. Org. Chem.*, 2019, 7635–7643.

14 A. Laventure, S. Stanzel, A.-J. Payne, B. H. Lessard and G. C. Welch, A Ring Fused N-Annulated PDI Non-Fullerene Acceptor for High Open Circuit Voltage Solar Cells Processed from Non-Halogenated Solvents, *Synth. Met.*, 2019, **250**, 55–62.

15 X. Tian, Y. Xiao, S. Wang, G. Liu, W. Zhang, L. Zhou, J. Gong, X. Zhang, X. Li, H. Meng, J. Wang, G. Dai and Q. Wang, Bowl-Shaped Bispyrrole-Fused Perylene-Diimide and Its Anions, *Org. Lett.*, 2023, **25**(10), 1605–1610.

16 S. Hayakawa, A. Kawasaki, Y. Hong, D. Uraguchi, T. Ooi, D. Kim, T. Akutagawa, N. Fukui and H. Shinokubo, Inserting Nitrogen: An Effective Concept To Create Nonplanar and Stimuli-Responsive Perylene Bisimide Analogues, *J. Am. Chem. Soc.*, 2019, **141**(50), 19807–19816.

17 K. Bartkowski, P. Zimmermann Crocomo, M. A. Kochman, D. Kumar, A. Kubas, P. Data and M. Lindner, Tandem Rigidification and π-Extension as a Key Tool for the Development of a Narrow Linewidth Yellow Hyperfluorescent OLED System, *Chem. Sci.*, 2022, **13**(34), 10119–10128.

18 X. Tian, K. Shoyama and F. Würthner, Nitrogen-Doped Polycyclic Aromatic Hydrocarbons by a One-Pot Suzuki Coupling/Intramolecular S_NAr Reaction, *Chem. Sci.*, 2023, **14**(2), 284–290.

19 H. Luo and J. Liu, Facile Synthesis of Nitrogen-Doped Nanographenes with Joined Nonhexagons via a Ring Expansion Strategy, *Angew. Chem., Int. Ed.*, 2023, **62**(21), e202302761.

20 G. A. Petersson, T. G. Tensfeldt and J. A. Montgomery, A Complete Basis Set Model Chemistry. III. The Complete Basis Set-Quadratic Configuration Interaction Family of Methods, *J. Chem. Phys.*, 1991, **94**(9), 6091–6101.

21 C. M. Cardona, W. Li, A. E. Kaifer, D. Stockdale and G. C. Bazan, Electrochemical Considerations for Determining Absolute Frontier Orbital Energy Levels of Conjugated Polymers for Solar Cell Applications, *Adv. Mater.*, 2011, **23**(20), 2367–2371.

22 N. G. Connelly and W. E. Geiger, Chemical Redox Agents for Organometallic Chemistry, *Chem. Rev.*, 1996, **96**(2), 877–910.

23 V. V. Pavlishchuk and A. W. Addison, Conversion Constants for Redox Potentials Measured versus Different Reference Electrodes in Acetonitrile Solutions at 25 °C, *Inorg. Chim. Acta*, 2000, **298**(1), 97–102.

24 Q. Zhang, H. Kuwabara, W. J. Potscavage, S. Huang, Y. Hatae, T. Shibata and C. Adachi, Anthraquinone-Based Intramolecular Charge-Transfer Compounds: Computational Molecular Design, Thermally Activated Delayed Fluorescence, and Highly Efficient Red Electroluminescence, *J. Am. Chem. Soc.*, 2014, **136**(52), 18070–18081.

25 L. Yao, S. Zhang, R. Wang, W. Li, F. Shen, B. Yang and Y. Ma, Highly Efficient Near-Infrared Organic Light-Emitting Diode Based on a Butterfly-Shaped Donor–Acceptor Chromophore with Strong Solid-State Fluorescence and a Large Proportion of Radiative Excitons, *Angew. Chem., Int. Ed.*, 2014, **53**(8), 2119–2123.

